Int. J. Electrochem. Sci., 11 **(2016)** 2106 - 2118

International Journal of
ELECTROCHEMICAL
SCIENCE
www.electrochemsci.org

Synthesis and Evaluation of Self-healing Cerium-Doped Chitosan Nanocomposite Coatings on AA5083-H321

Hossein Hassannejad[*] *and Ashkan Nouri*

Department of Materials Science and Metallurgy, Faculty of Engineering, Arak University, Arak, Iran.
[*]E-mail: H-Hasannejad@araku.ac.ir

Received: 4 December 2015 / *Accepted:* 29 December 2015 / *Published:* 1 February 2016

The effect of cerium ion and CeO_2 nanoparticles on the formation and corrosion behavior of self-healing CeO_2-chitosan (CeO_2-CHIT) nanocomposite coatings on AA5083-H321 was studied by SEM, TEM, XPS, FTIR, potentiodynamic polarization and electrochemical impedance spectroscopy. High corrosion resistance coating was obtained when the cerium ion concentration in the chitosan (CHIT) films was 5 mM. It has been observed that the presence of $5gr.lit^{-1}$ CeO_2 nanoparticles in the CHIT coatings doped with cerium ions (CHIT-CE) provided higher corrosion resistance. This coating showed high impedance after the 12 hours of immersion in 3.5% NaCl. With further increase in immersion time from 12 to 24, 48 and 72 hours, this trend continued to increase in corrosion resistant. The progressive increase in the impedance values of CeO_2-CHIT-Ce (5 mM) coatings with increasing time of immersion showed that this coating exhibits 'self-healing" type behavior.

Keywords: Self-Healing, Aluminum alloys AA5083-H321, Chitosan, Cerium oxide, Nanocomposite

1. INTRODUCTION

Natural oxide film on aluminum alloy does not give enough protection against aggressive anions, so inhibitors and coatings are used to improve protective features of its surface [1-2]. The most common and cost-effective method of improving the corrosion resistant of the aluminum alloy, is using of coatings. In the corrosion protection system, the main task of the coating is to offer a dense barrier against aggressive anions. During operation of the coated structures, defects disappear in the coating which allowing direct access of aggressive anions to the aluminum surface. Thus, corrosion accelerates after disruption of the protective layer. Therefore, it is essentially to offer long-term protection active 'self-healing' of defects in the films [3-5].

In the past, the most effective system to protect of aluminum alloys from active corrosion process has contained chromates. Leachability and high oxidation potential of chromate provided self-

healing anticorrosion coatings and excellent corrosion protection. Unfortunately, reports have shown that chromium (VI) is a carcinogen, and can cause kidney and liver damage, and even death. Hence, in the last decade research efforts have focused on the use of environmentally friendly materials obtained from renewable resources [3-6].

The standard accepting of self-healing coating is the complete recovery of the coating to restores the first integrity of it due to real healing of the defect. On the other hand, the main purpose of anticorrosive coatings is protection of a metallic substrate against aggressive anions attack. Thus, the recovery of coating integrity is not obligatory and self-healing of anticorrosive protective films can get by incorporating of corrosion inhibitors into the coating system [7-10].

In this context, chitosan coatings have been widely considered as a candidate because of its specific properties such as good film-forming ability, biocompatibility, nontoxicity, biodegradability and antibacterial activity [11-14].

Recently, Carneiro et al [15] worked on active chitosan-based films containing corrosion inhibitors. In this case, the chitosan film was applied before deposition of a barrier films as a corrosion inhibitor tank pre-layer. In the present work, the environmentally friendly and self-healing CeO_2-CHIT-CE nanocomposite coatings were deposited on AA5083-H321. CHIT was used as a repository of inhibitor maintenance in advance before applying the hybrid layer and different cerium nitrate concentrations (1, 5 and 10mM) were used as inhibitor. For considering the effect of cerium oxide nanoparticles, CeO_2 nanoparticles were dispersed into CHIT film to form CeO_2-CHIT-CE nanocomposite coating. Corrosion and self-healing properties of CeO_2-CHIT-CE nanocomposite coating were assessed by potentiodynamic polarization and electrochemical impedance spectroscopy.

2. MATERIALS AND METHODS

2.1. Preparation of samples

In this research aluminum alloys AA5083-H321 which the composition are shown in Table. 1 was used for test. Pretreatment is an important procedure before coating, sample was degreased with acetone and rinsed with deionized water completely. Then the sample was degreased with alkaline cleaner (NaOH). Prior coating process, specimen was rinsed thoroughly with deionized water.

Table 1. Chemical composition of AA5083-H321 aluminum–magnesium alloy.

Element	Mg	Si	Mn	Cr	Fe	Cu	Zn	Ti	Al
Wt.%	4.6	0.2	0.8	0.09	0.7	0.28	0.05	0.05	Balance

2.2. Deposition process

Solutions were prepared by dissolving of 1 wt% chitosan flakes (85% deacetylated) in a 1%(v/v) acetic acid aqueous solution by magnetic stirring at room temperature for 24 h. Different

concentrations of inhibitor ($Ce(NO_3)_3$:1, 5 and 10 mM) were added and stirred for 12 h to reach total dissolution. The CHIT-CE films were obtained by dip immersion method, in this process samples were immersed into and withdrawn from the solutions with a constant speed of 8 cm/min and dried before the deposition of the next layer, until 5 layers were obtained. For investigating the effect of ceria nanoparticles, the calculated amount of CeO_2 nano particles (The average particle size of the CeO_2 powder was 20 nm.) were dispersed in the CHIT-CE solution by stirring at room temperature (25 °C) then it was sonicated for 1hr. Cerium oxide was deposited on CHIT-CE coatings by sol-gel method to study the effect of last hybrid layer. The sol of cerium oxide was prepared by mixing ceric ammonium nitrate in ethanol. The mixture stirred at room temperature for 30 min. After that, small amount of distilled water was added to the mixture to accelerate hydrolysis and condensation. In the next step, the suspension stirred for 10 h until it turns to a clear solution. The prepared sol was aged for 8 days at room temperature with humidity of (50±5%) and the last film was formed by dip immersion, and dried in the oven at 100℃ for 24 hours.

2.3. Examination of coatings

The corrosion behavior of the coatings was investigated using polarization techniques and electrochemical impedance spectroscopy (EIS); during immersion in 3.5% wt NaCl, with a potentiostat/ galvanostat (IVIUMSTAT). Potentiodynamic polarization was applied with a scan rate of 0.6mV/s and EIS was performed between 10 m Hz and 100 k Hz frequency ranges and the impedance plots were fitted using Iviumsoft software. The surface morphology and chemical composition of the coatings were examined by SEM (XL-30 (PHILIPS)), TEM (JEOL JEM 200CX) and X-ray photoelectron spectroscopy (XPS). The XPS analysis was performed on a PHI-5700 ESCA system using an Al Ka (1486.6 eV) X-ray source. Fourier transform infrared spectra were obtained on a Perkin-Elmer Model BX2 spectrometer with resolution of 1 cm^{-1}.

3. RESULT AND DISCUSSION

3.1. Characterization of CHIT, CHIT-CE and CeO_2-CHIT-CE nano composite coatings

Fig. 1 shows the chemical bonding structures of the CHIT, CHIT-CE and CeO_2-CHIT-Ce coatings. Data on the pure chitosan, CHIT-CE and CeO_2-CHIT+Ce coatings are presented for comparison. Fig. 1a indicates FTIR spectrum of pure CHIT film. In the wave number region of 3442 cm^{-1}, the axial stretching vibrational mode of O-H and NH_2 groups is observed. Bands centered at 2850 and 2920 cm^{-1} corresponding to the symmetric or asymmetric C-H and CH_2 stretching vibration. In addition, peaks appear at 1588, 1428, 1633 and 1452cm^{-1} related to amide bands and the bands at 1122, 1053 and 883 cm^{-1} are due to the C-O and C-O-C stretching [15-17].

Fig. 1b presents the FTIR spectra of CHIT-CE (1, 5mM) and CeO_2–CHIT-CE nanocomposite coatings. The bands of CHIT corresponding to the OH and NH_2 groups stretching modes become sharper and broader in the IR spectra of CHIT-CE and CeO_2-CHIT-CE coatings. This result shows the

assembly of CHIT with $Ce(NO_3)_3$ and nano CeO_2 in the NH_2/OH group [15-18]. In addition, the bands at ~ 1433, ~ 1539 cm^{-1} become wider, and the intensity of them increase. This variation probably related to process of complexation that occurs between Ce^{3+} and the amine group [15-18]. By adding $Ce(NO_3)_3$ and nano CeO_2 particles to CHIT, a notable IR band at ~595 cm^{-1} is observed which related to Ce–O stretching vibration mode [15-18]. In addition, a new band is observed at wave number (~460 cm^{-1}) in the IR spectra of CeO_2-CHIT-CE nanocomposite film, corresponding to pure nano CeO_2 [19-20].

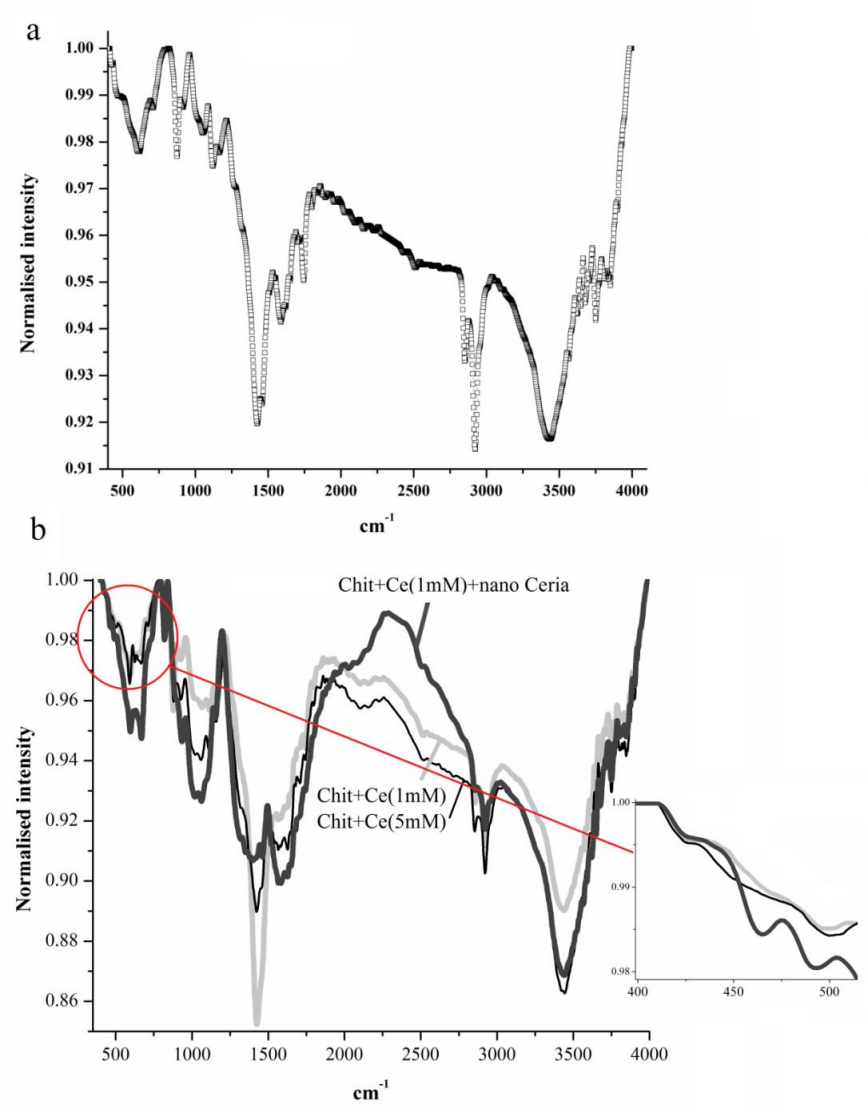

Figure 1. FTIR spectrum of CHIT (a), CHIT-CE and CeO_2-CHIT-CE (b) coatings on AA5083-H321.

3.2. Corrosion resistance

Fig. 2 presents the polarization curves of the CHIT and CHIT-CE (1, 5 and 10 mM) coatings after a 1 hr immersion in 3.5% NaCl solution. It shows that the corrosion potential of the CHIT-CE coatings shifts to more negative potentials with lower current density compared to aluminum alloy and

pure CHIT film. This illustrates the cathodic inhibition mechanism of cerium ions in the coatings [21-23].

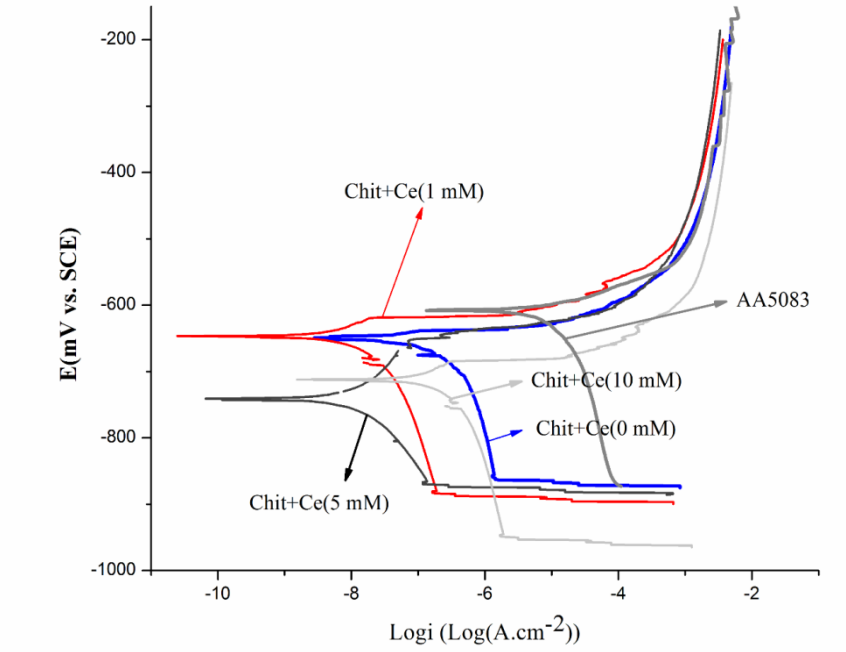

Figure 2. Polarization curves of the CHIT and CHIT-CE (containing different concentration of Ce ions) films after 1 h immersion in 3.5% NaCl solutions.

Table 2. Values of i_{corr},R_p , E_{corr}, E_{pit} and E_{pit}-E_{corr} obtained from potentiodynamic scan (Fig.2)

	E_{corr}(mV)	i_{corr}(A/cm^2)	E_{pit} (mV)	E_{pit}-E_{corr} (mV)	R_P(k ohms)
AA5083-H321	-609	1.25×10^{-5}	———	0	28.342
Chit+0 mM Ce(III)	-654	3.98×10^{-7}	———	0	98.558
Chit+1 mM Ce(III)	-644	3.98×10^{-8}	-601	43	393.379
Chit+5 mM Ce(III)	-737	1.99×10^{-8}	-623	115	684.234
Chit+10 mM Ce(III)	-712	3.16×10^{-7}	-668	44	96.723

Table 2 tabulates corrosion current densities (i_{corr}), corrosion potential (E_{corr}) and passive region (E_{pit}–E_{corr}) of the CHIT and CHIT-CE coatings. The results show that by increasing the cerium ion concentration in CHIT films, the values of polarization resistance increase considerably. Extremely high corrosion resistance is obtained when the cerium ions concentration in the CHIT films is 5 mM. Corrosion inhibition mechanism of cerium ions probably is the main reason of this increase in the corrosion resistance. Cerium inhibits corrosion through a change of valence from +3 to +4 on the surfaces of the coatings [24].

The results show that higher concentrations of cerium ions could induce defects formation and cracks in the CHIT coating, decreasing the barrier properties (Fig. 3). The presence of cracks in the CHIT films is mainly due to formation of cerium oxide or cerium hydroxide in the CHIT coating as mentioned before in the FTIR results. In fact, there is a critical concentration for beneficial effects of cerium ions on the corrosion resistance of CHIT coating. Higher concentrations of cerium ions decrease the resistance of the coating due to high expansion coefficient of cerium oxide which can strengthen the probability of cracking [24].

Fig. 4a displays the polarization curves of the optimum coating (CH-CE (5 mM) film) with and without the final hybrid layer. By depositing the hybrid layer, both of the corrosion resistance and the passive region decrease. These decreasing probably related to the cracks formation in the hybrid layer (Fig. 4b). In the CHIT-CE(5mM) film, when the coating is exposed to the solution the cerium ion through a change of valence from +3 to +4 on the surfaces formed a new layer of cerium oxide on the outer surface of the coating [24]. This uniform and crack-free film acts as barrier coating on CHIT-CE films that shows better anticorrosion behavior compare to ultimate hybrid layer.

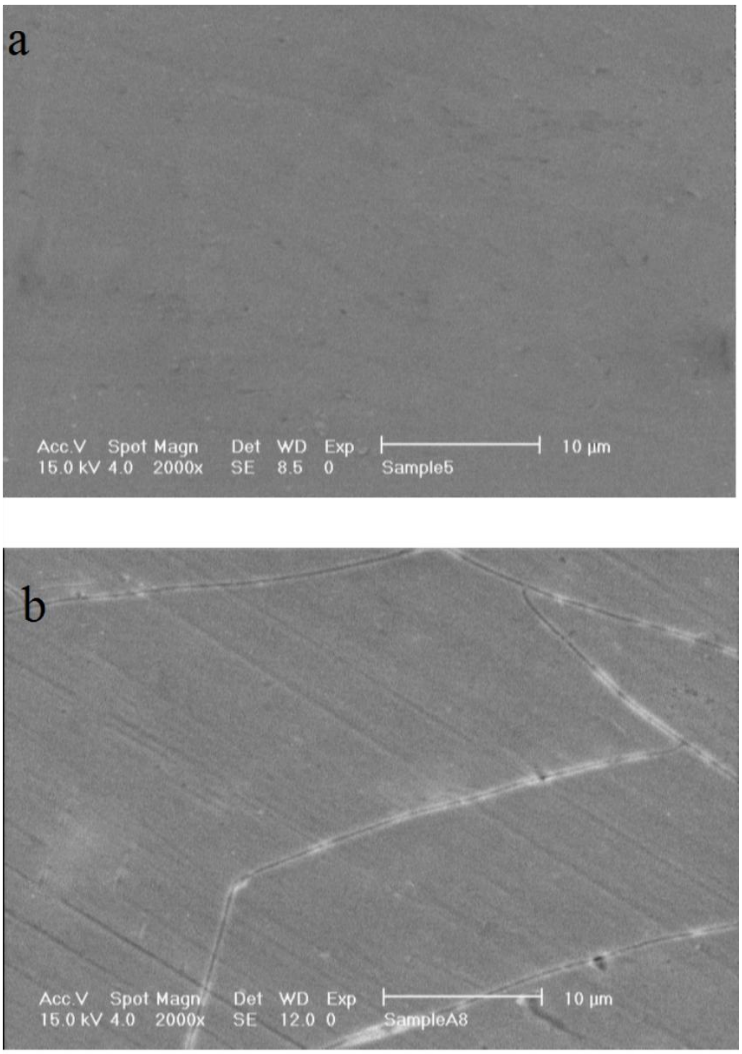

Figure 3. SEM images of chitosan film doped with 5 mM ion (a) and 10 mM Ce(III) (b).

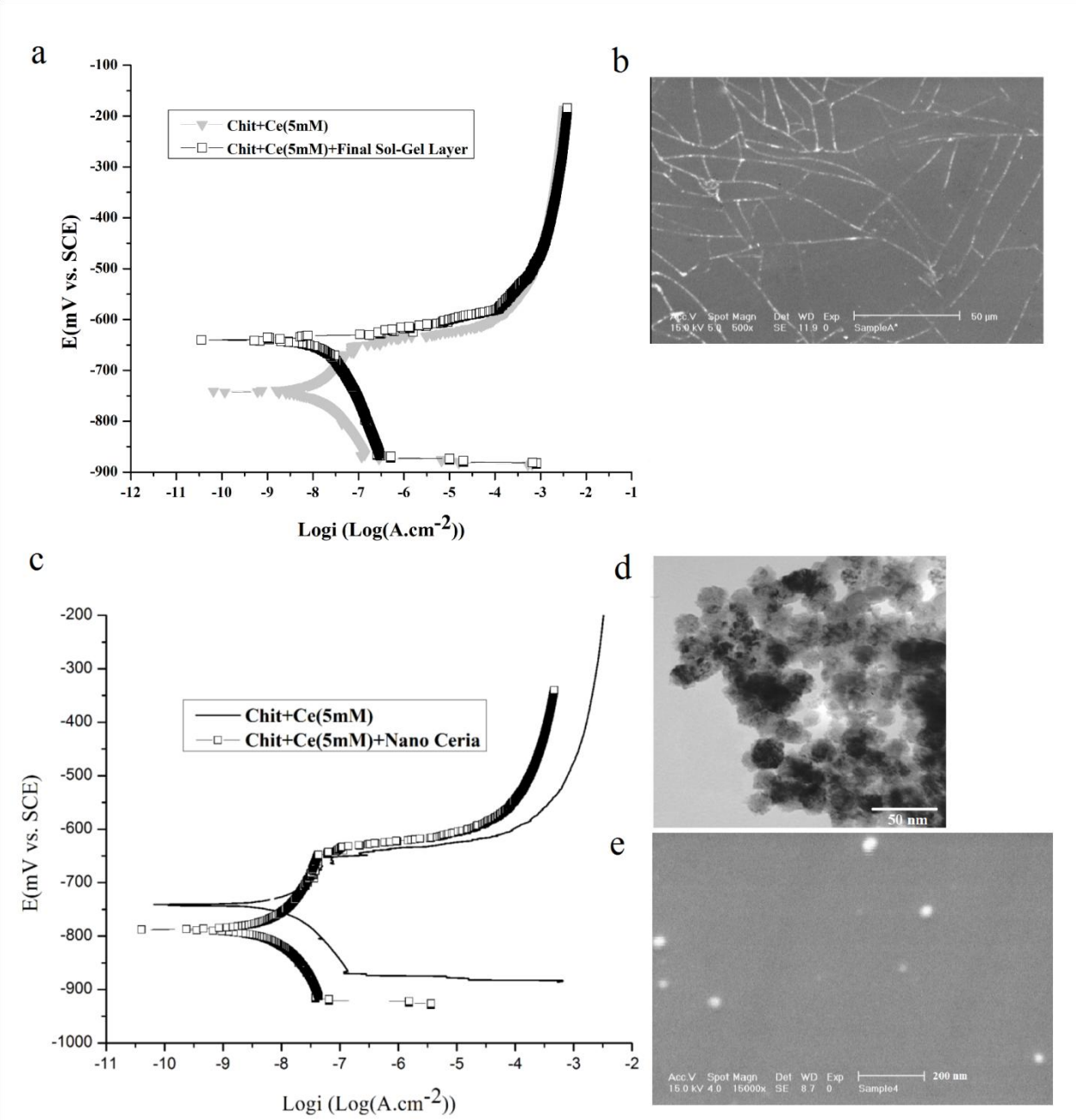

Figure 4. (a) Polarization curves of the CHIT-Ce(5mM) films with and without the final hybrid layer and (c) Polarization curves of CeO_2-CHIT-Ce(5mM) films in 3.5% NaCl solution. (b) SEM images of hybrid layer on CHIT-CE films and (d,e) SEM and TEM images of CeO_2 nanopowder and CeO_2–CHIT-CE films.

3.3. Effect of ceria nanoparticles

To consider the effect of ceria nanoparticles, 5 $gr.lit^{-1}$ of CeO_2 nanoparticles were added into CHIT-CE (5 mM). Fig. 4c shows the potentiodynamic curves of CHIT-CE and CeO_2-CHIT-CE nanocomposite coatings. By addition of CeO_2 nanoparticles, the corrosion resistance of the coating increased. Intermetallic components in the aluminum alloys are the main reason for pitting. Figures 4d and 4e present the TEM image of CeO_2 nanoparticles and the SEM image of CeO_2- CHIT-CE

nanocomposite coating. CeO_2 nanoparticles dispersed adequately in the CeO_2- HITCE coating. In consequence, the potential of the coating become uniform and positive and the potential differential between intermetallic components and substrates is neglected.

3.4. EIS measurement

Fig. 5 shows the Nyquist and Bods plots of CHIT, CHIT-CE and CeO_2-CHIT-CE nanocomposite coatings in 3.5% NaCl. CHIT-CE coatings show better barrier properties compare to the pure chitosan and the most effective corrosion protection performance was obtained when the concentration of $Ce(NO_3)_3$ was 5 mM. Furthermore, addition of 5gr.lit^{-1} CeO_2 nanoparticles into CHIT-CE film make a considerably enhancement in the corrosion resistance of the coating. For quantitatively estimation of the electrochemical properties of CHIT and CHIT-CE and CeO_2- CHIT-CE nanocomposite coatings, experimental impedance spectra were fitted using equivalent circuits (Fig 6). These model parameters are as follows: R_s is the solution resistance, R_{coat}: coating resistance, R_{ct}: charged transfer resistance of corroded areas, CPE_{coat}: the constant phase element of the coating and CPE_{dl} is the constant phase element of double layer. Table 3 shows the fitted data for the above-mentioned model.

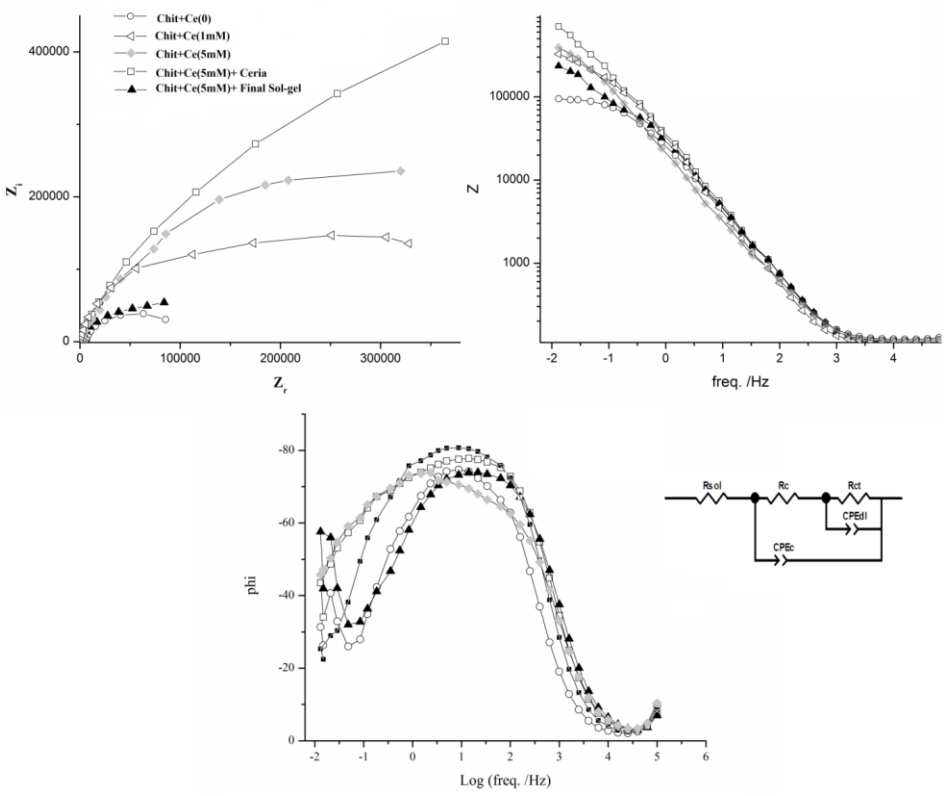

Figure 5. Nyquist and Bods plots of CHIT, CHIT-CE and CeO_2-CHIT-CE films after 1 hr immersion in 3.5%NaCl and equivalent electrical circuit (depicted in the same figure).

By adding cerium ions into CHIT film, the R_{ct} values of the coatings increased which prove the potentiodynamic analyses. It is probably related to the surface modification and inhibitory effect of cerium ions. CeO_2-CHIT-CE (5 mM) nanocomposite coating shows the highest amount of charge transfer resistance while the amount of double layer capacity in it is the lowest. The R_{ct} values obtained from EIS are comparable with the polarization resistance (R_p) values obtained from polarization tests. Table 3 shows that by increasing the cerium ion concentration in the CHIT films, the value of R_{coat} and the value of CPE_{coat} increased and decreased, respectively which confirm the potentiodynamic results.

Table 3. Fitting parameters for the EIS data using the proposed equivalent circuits for Ni and Ni–cerium oxide composite coatings

Coatings	$R_{sol}(\Omega)$	$R_c(\Omega)$	$R_{ct}(\Omega)$	$CPE_c(e^{-6}F)$	n_c	$CPE_{dl}(e^{-5}F)$	n_{dl}
CH	32	85442	98342	9.13	0.78	5.77	0/74
CH-Ce(1mM)	42	184876	376543	6.04	0. 81	4.43	0/69
CH-Ce(5mM)	28	272231	453423	2.8	0.84	3.27	0/84
CH-Ce(5mM)+Ceria	45	382405	786185	0.87	0.92	3.1	0/67
CH-Ce(5mM)+Hybrid	51	124232	309865	4.59	0.71	4.39	0/72

Furthermore, by applying the hybrid layer on the CHIT-CE coating the values of R_{coat} and the values of CPE_{caot} increase and decrease, respectfully. This decrease in barrier properties probably related to the nature of the hybrid layer that contained cracks and defects. In addition, Table 3 shows a decrease in the value of n_{coat} which is an indicator of surface roughness. The presence of cracks and defects in the sol–gel layer are the mainly reason for this undesirable effect. By adding CeO_2 nanoparticles to the CHIT-CE film, the highest value of R_{coat} and the lowest value of CPE_{coat} are obtained.

3.5. Evaluation of self-healing properties

The electrochemical response of CeO_2-CHIT-CE (5mM) nanocomposite coating was evaluated using EIS within a 3.5% NaCl solution for 120 hours (Fig. 6). However, the value of impedance for coated AA5083-H321 decreases with increasing time of immersion from beginning to 12 hours. This coating shows high impedance after 72 hours of immersion. In the time range from 12 to 120 hours, a progressive increase in impedance values is noticeably detectable. This tendency shows that CeO_2-CHIT-CE (5 mM) coating displays a self-healing ability. The higher values of impedance after such a long exposure to the aggressive solution confirmed the superior corrosion resistance of the CeO_2-CHIT-CE nanocomposite coating.

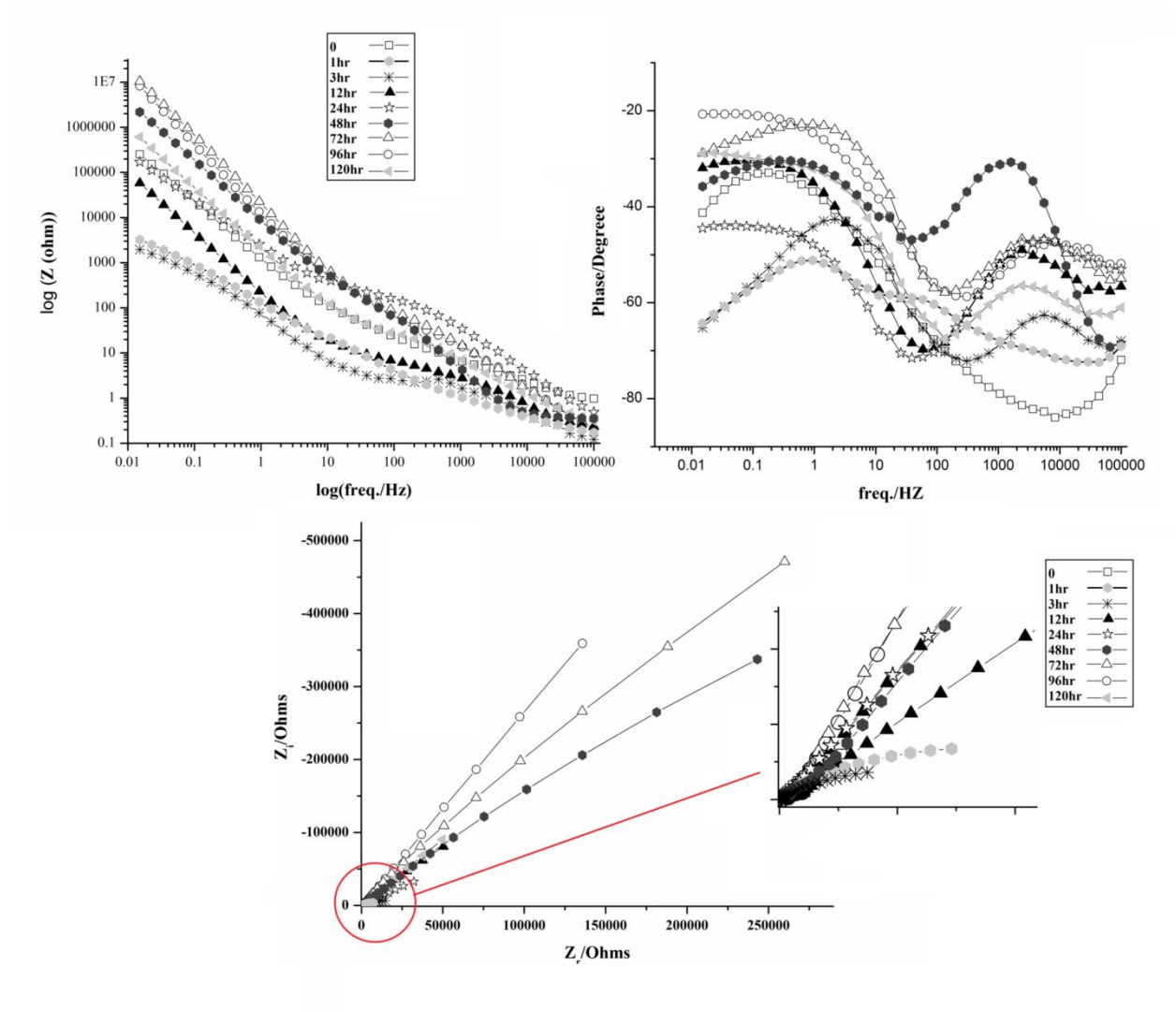

Figure 6. EIS spectra for AA5083 coated with CeO_2-CHIT-Ce (5mM) after 120hr immersion in 3.5% NaCl solution.

In high frequency region, after 3 hours of immersion a new time constant is observed in the Bods curves. High frequency region in impedance spectroscopy gives a detail about the behavior of outer layer. The aforementioned results show that the new layer was formed on the outer surface of the coating. This thin layer, associated with the formation of non-stoichiometric cerium oxide layer. XPS analyse was used to study the chemical composition of the cerium oxide in the CHIT-CE coatings. Fig. 7 presents XPS spectra of Ce 3d regions for CHIT-CE film before and after 48 hours of immersion in 3.5% NaCl solution. XPS spectrum shows six peaks [25-27], which related to Ce (IV) and Ce (III). The cerium oxide exists as mixture of the Ce (IV) and Ce (III). The Ce (IV) / Ce (III) ratio in the CHIT-CE coatings before immersion is about 1.24. However, after 48 hours immersion this ratio increases and reaches to 2.07.

These result shows that during immersion of samples in the 3.5% NaCl solution, cerium ions released from the chitosan coating and due to the cathodic reactions on the surface and increase of local pH $Ce(OH)_3$ or soluble $Ce(OH)_2^{2+}$ complexes are formed (Equation 1-2) [28-29].

(1) $Ce^{3+} + 3OH^- \rightarrow Ce(OH)_3$

(2) $Ce^{3+} + 2OH^- \rightarrow Ce(OH)_2^{2+} + e^-$

Then cerium oxide film obtains from the oxidation of cerium hydroxide (Equation (3)) or from the hydrolysis of $Ce(OH)_2^{2+}$[28-29].

(3) $Ce(OH)_3 \rightarrow CeO_2 + H_3O^+ + e^-$

(4) $Ce(OH)_2^{2+} + 2OH^- \rightarrow CeO_2 + 2H_2O$

Corrosion inhibition properties of cerium might be the main reason for the repair of defect in the chitosan films. In conclusion, cerium ions in the chitosan coating diffuse through localized defects and when placed in contact with the solution, inhibits corrosion through a change of valence from +3 to +4 on the surface and formation of a thin layer of cerium oxide. By forming the cerium oxide or cerium hydroxide layer, the self-healing properties of the coatings continue.

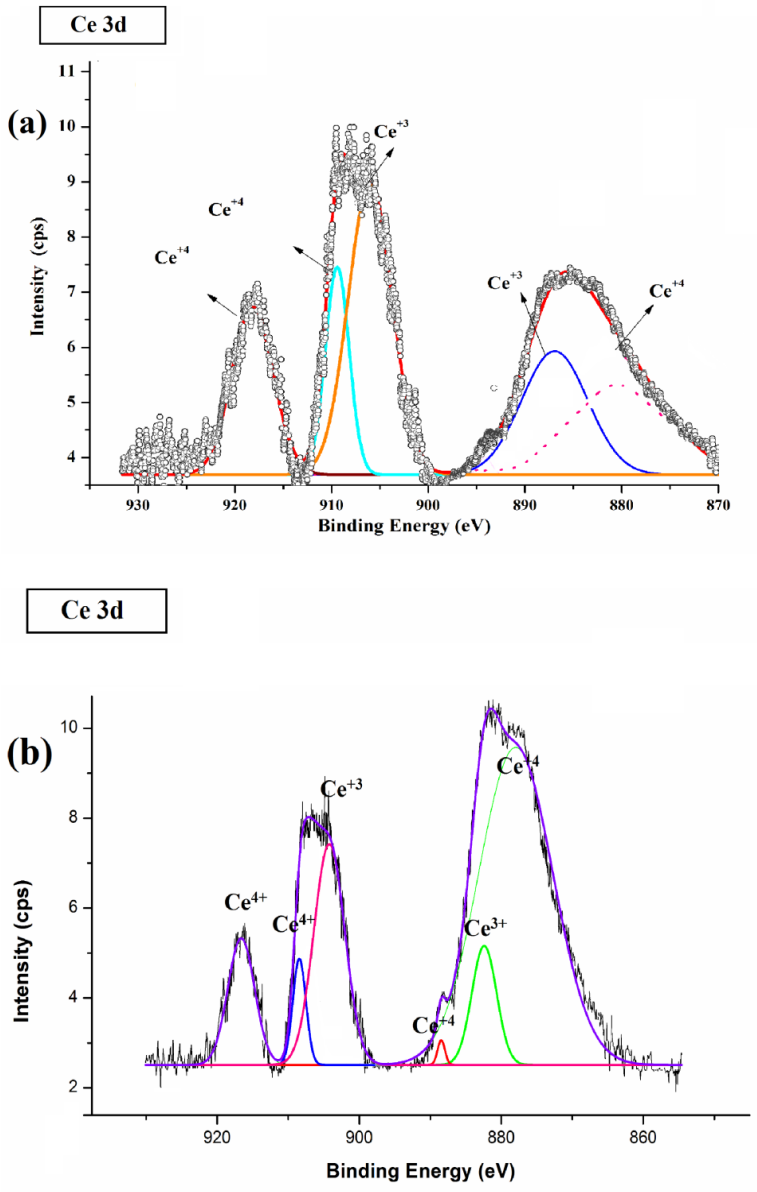

Figure 7. High-resolution X-ray photoelectron spectra (XPS) of the Ce 3D region for CHIT-CE film before (a) and after (b) 48hrs of immersion in NaCl.

4. CONCLUSIONS

In this research, the environmentally friendly and self-healing CeO_2-CHIT-CE nanocomposite coatings were prepared on AA5083-H321 by dip immersion. By increasing the cerium ion concentration in CHIT films, the corrosion resistance of the coatings increase extensively. Extremely high corrosion resistance is obtained when the cerium ions concentration in the CHIT films is 5 mM. Higher concentrations of cerium ions could induce the formation of defects in the CHIT coating, decreasing the barrier properties. Addition of $5gr.lit^{-1}$ CeO_2 nanoparticles into CHIT-CE film make a considerably enhancement in the corrosion resistance of the coating. The results of EIS show the progressive increase in the impedance values of CeO_2-CHIT-Ce (5 mM) coatings with increasing time of immersion. This tendency proves that CeO_2-CHIT-CE nanocomposite coating displays a self-healing ability. In conclusion, the results show that cerium ions in the chitosan coating diffuse through localized defects and when placed in contact with the solution, inhibits corrosion through a change of valence from +3 to +4 on the surface and formation of a thin layer of cerium oxide.

References

1. X. Zhong, X. Wu, Y. Jia and Y. Liu, *Appl. Surf. Sci.*, 280 (2013) 489
2. S. Jain, J.L. Hudson and J.R. Scully, *Electrochim. Acta*, 108 (2013) 253
3. H. Rahimi, R. Mozaffarinia and A.H. Najafabadi, *J. Mater. Sci. Technol.*, 29 (2013) 603
4. H.D. Johansen, C.M.A. Brett and A.J. Motheo, *Corros. Sci.*, 63 (2012) 342
5. D. Ghosh, A.K. Shukla and S.K. Mitra, *Surf. Eng.*, 29 (2013) 584
6. W. Zhang, J.Q. Li, Y.S. Wu, J.T. Xu and K. Chen, *Surf. Eng.*, 18 (2002) 224
7. K.A. Yasakau, J. Tedim, M.L. Zheludkevich and M.G.S. Ferreira, "Smart self-healing coatings for corrosion protection of aluminium alloys", Handbook of Smart Coatings for Materials Protection, 2014
8. B.L. Lin and J.T. Lu, *Trans. Nonferrous Met. Soc. China*, 24 (2014) 2723
9. H. W. Shi, F.C. Liu and E.H. Han, *Trans. Nonferrous Met. Soc. China*, 20 (2010) 1928
10. K. Zuo, X. Wang, W. Liu and Y. Zhao, *Trans. Nonferrous Met. Soc. China*, 24 (2014) 1474
11. P. Li, X. Zhang, R. Xu, W. Wang, X. Liu, K.W.K. Yeung and P.K. Chu, *Surf. Coat. Tech.*, 232 (2013) 370.
12. J. Carneiro, J. Tedim, S.C.M. Fernandes, C.S.R. Freire, A. Gandini, M.G.S. Ferreira and M.L. Zheludkevich, *Surf. Coat. Tech.*, 226 (2013) 51
13. M.P. Neupane, I.S. Park and M.H. Lee, *Thin Solid Films*, 550 (2014) 268
14. A.A. Rasha, A.F. Sahar, E. Nader and M.F.G. Sanaa, *Appl. Surf. Sc.i*, 292 (2014) 390
15. J. Carneiro, J. Tedim, S.C.M. Fernandes, C.S.R. Freire, A.J.D. Silvestre, A. Gandini, M.G.S. Ferreira and M.L. Zheludkevich, *Prog. Org. Coat.*, 75 (2012) 8
16. X. Tan, M. Li, P. Cai, L. Luo and X. Zou, *Anal. Biochem.*, 337 (2005) 111
17. B.D. Malhotra and A. Kaushik, *Thin Solid Films*, 518 (2009) 614
18. M. Cai, L. Zhu, Y. Ding, J. Wang, J. Li and X. Du, *Mater. Sci. Eng* C, 32 (2012) 2623
19. A. Vermaa, A.K. Bakhshib and S.A. Agnihotry, *Sol. Energ. Mat. Sol*. C, 90 (2006), 1640
20. T. Yoshino and H. Masuda, *Solid State Ionics*, 165 (2003)123
21. F. Deflorian, M. Fedel, S. Rossi, *Electrochim. Acta*, 56 (2011) 7833
22. D. Zhao, J. Sun, L. Zhang, Y. Tan and J. Li, *J. Rare. Earth*, 28 (2010) 371
23. M.L. Zheludkevich, R. Serra, M.F. Montemor, K.A. Yasakau, I.M. Salvado and M.G.S. Ferreira, *Electrochim. Acta*, 51 (2005) 208

24. H. Hassannejad, T. Shahrabi, F. Malekmohammadi, A. Shanaghi, M. Aliofkhazraei and A. Oskuie, *Curr. Appl. Phys*., 10 (2010) 1022
25. X. Huang, N. Li, H. Wang, H. Sun, S. Sun and J. Zheng, *Thin Solid Films*, 516 (2008)1037
26. P. Stefanov, G. Atanasova, D. Stoychev and T.S. Marinova, *Surf. Coat. Tech*,, 180 (2004) 446
27. D.R. Mullins, S.H. Overbury and D.R. Huntley, *Surface Science*, 409 (1998) 307
28. Y. Hamlaoui, F. Pedraza, C. Remazeilles, S. Cohendoz, C. Rebere, L. Tifouti and J. Creus, *Mater. Chem. Phys*,, 113 (2009) 650
29. S.A. Hayes, Y. Pu, J.T. O'Keefe, J.M. O'Keefe and J.O. Stoffer, *J. Electrochem. Soc*., 149 (2002) 623.